



LJMU Research Online

Esen, AF, Woodward, PK, Laghrouche, O, Cebasek, TM, Brennan, AJ, Robinson, S and Connolly, DP

Full-Scale Laboratory Testing Of A Geosynthetically Reinforced Soil Railway Structure

<http://researchonline.ljmu.ac.uk/id/eprint/14609/>

Article

Citation (please note it is advisable to refer to the publisher's version if you intend to cite from this work)

Esen, AF, Woodward, PK, Laghrouche, O, Cebasek, TM, Brennan, AJ, Robinson, S and Connolly, DP (2021) Full-Scale Laboratory Testing Of A Geosynthetically Reinforced Soil Railway Structure. Transportation Geotechnics. 28. ISSN 2214-3912

LJMU has developed [LJMU Research Online](#) for users to access the research output of the University more effectively. Copyright © and Moral Rights for the papers on this site are retained by the individual authors and/or other copyright owners. Users may download and/or print one copy of any article(s) in LJMU Research Online to facilitate their private study or for non-commercial research. You may not engage in further distribution of the material or use it for any profit-making activities or any commercial gain.

The version presented here may differ from the published version or from the version of the record. Please see the repository URL above for details on accessing the published version and note that access may require a subscription.

For more information please contact researchonline@ljmu.ac.uk

<http://researchonline.ljmu.ac.uk/>

FULL-SCALE LABORATORY TESTING OF A GEOSYNTHETICALLY REINFORCED SOIL RAILWAY STRUCTURE

A.F. Esen¹, P.K. Woodward², O. Laghrouche¹, T. M. Čebašek², A.J. Brennan³, S. Robinson³,
D.P. Connolly²

¹Institute for Infrastructure and Environment, Heriot-Watt University, Edinburgh EH14 4AS, UK

²Institute for High-Speed Rail and System Integration, University of Leeds, Leeds LS2 9JT, UK

³School of Science and Engineering, University of Dundee, Dundee DD1 4HN, UK

Abstract

Railway lines typically use traditional sloping embankments as the principal means of track support. However, the use of Geosynthetically Reinforced Soil (GRS) systems have gained popularity as alternatives to conventional embankments, particularly for high-speed lines in Japan. This system requires less ground stabilization/improvement and less land take than conventional embankments due to its smaller base area. This research investigates the immediate and long-term settlement behaviour of a Geosynthetically Reinforced Soil with Retaining Wall (GRS-RW) system subject to cyclic loading for two track forms: a concrete slab track and a ballasted track. First, a three-sleeper concrete slab section is constructed at full-scale under controlled laboratory conditions, followed by a ballasted track. Both are supported on a 1.2m deep subgrade and a frost protection layer in accordance with railway design standards. Two different axle load magnitudes are applied statically, and then cyclically/dynamically, using 6 actuators to replicate moving train axle loads. It is observed that the slab track performs significantly better in terms of elastic and plastic deformation under both static and cyclic loading. Overall, the amplitude of the rail displacement under an individual cycle loading was approximately 25% lower for the slab track and the amplitude of the sleeper displacement on the ballasted track was approximately 6-7 times higher.

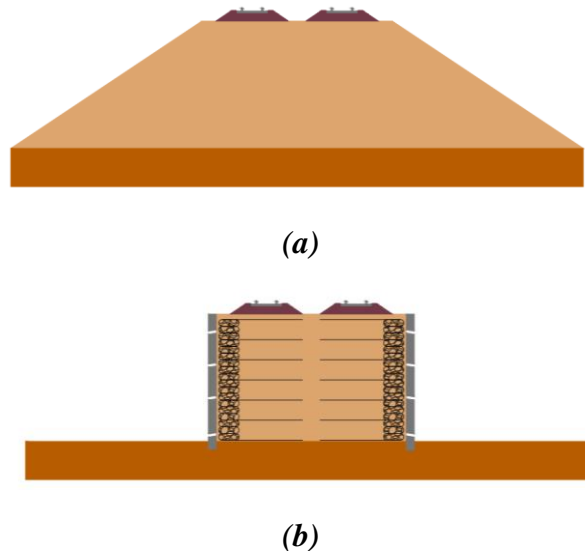
Keywords: *Full-scale cyclic loading; Railway track settlement; Geosynthetically Reinforced Soil; Long-term rail track behaviour; Ballast and concrete slab track; Railway Embankment*

1 Introduction

The growing demand for rail lines leads railway infrastructure companies to trim the life-cycle costs of railways due to increasing economic pressures. This is particularly true for high-speed lines but equally applicable to conventional-speed lines. In addition to the ongoing discussion on the performance of the ballasted and the ballastless (slab) tracks, alternative types of track support structures are also being proposed to improve the inherent track quality while lowering the upfront capital construction costs.

Geogrids are proven to be a practical solution used under the ballast to reduce the permanent deformation for railways (Yu, et al., 2019; Singh, et al., 2020; Punetha, et al., 2020). In the last

38 decades, geosynthetically reinforced soils (GRS) emerged as a reliable transportation
39 infrastructure mitigation strategy. GRS structures have been constructed extensively at various
40 infrastructures along highways, particularly at bridge abutments all over the world (Lee & Wu,
41 2004; Lenart, et al., 2016; Berg, et al., 2009; Wu, 2018; Herold, 2005; Helwany, et al., 2003;
42 Skinner & Rowe, 2005; Kim & Kim, 2016). Embankments have been used as the principal
43 means of supporting the railway track for nearly 200 years (Connolly, et al., 2013). Indeed,
44 modern high-speed railway lines still typically use traditional sloping embankments for track
45 support over flood plains and for route and track geometry considerations (e.g. China and
46 Europe) (Connolly, et al., 2014). However, in Japan, the application of geosynthetically
47 reinforced soil substructures in combination with retaining walls (GRS-RW) have gained
48 popularity as alternatives to conventional embankments, particularly for high-speed lines like
49 the Hokkaido Shinkansen, which is an extension from the high-speed lines from Tokyo
50 (Yonezawa, et al., 2014). A construction system of geosynthetic-reinforced soil (GRS) with
51 full height rigid (FHR) facing retaining walls (RWs) is now widely used in Japan. The total
52 length was more than 180km in 2018 (Tatsuoka, 2019).



57 **Figure 1:** Land occupation of; (a) a conventional embankment, and (b) GRS-RW system

58 These structures provide cost-effective solutions since they require less ground
59 stabilization/improvement (Dong, et al., 2018) and land take than conventional embankments
60 with a much smaller base area (**Figure 1**). They also provide lower residual displacements
61 during operation, i.e. better operational performance than conventional embankments. A large
62 number of field investigations have been conducted to provide design methodology for
63 materials, and construction steps to build a GRS-RW structure for high-speed railways (Horii,
64 et al., 1994; Koseki, et al., 1996; Tatsuoka, et al., 1997; Koseki, et al., 2006; Tatsuoka, et al.,
65 2007; Koseki, 2012; Tatsuoka, et al., 2014; Yonezawa, et al., 2014; Tatsuoka, 2019; Tatsuoka
66 & Watanabe, 2015). Overall, structural stability is provided by the retaining walls, backfill and
67 the geosynthetics wrapped around gravel bags located directly behind the retaining walls. In
68 addition, reinforced-soil walls are generally more flexible than conventional retaining

69 structures. Thus, they may be used in areas where large uneven displacements are expected due
70 to surface movements during earthquake events.

71 The GRS-RW also takes advantage of full-height-rigid facing (FHR) which allows better
72 control over concentrated loads – an area that is particularly beneficial in railway applications.
73 Typical reinforced wall structures that use discrete wall panels can suffer severe damage if
74 there is a loss of stability of one of the panels. This, obviously, causes significant concerns and
75 issues for railways. The minimum specified FHR facing concrete thickness for GRS-RW is
76 30cm, which is based on constructability considerations. The facing is therefore very thin and
77 the required amount of steel-reinforcement in the facing is minimal. This thickness is typically
78 larger than that based on structural requirements. The maximum height of a GRS retaining wall
79 (with FHR facing) is recorded as 11m, while the tallest GRS bridge abutment is 13.4m high
80 (Tatsuoka, et al., 2014). Care needs to be taken at low wall heights to prevent a lack of confining
81 pressure causing active stability issues, hence the use of the gravel bags to provide lateral
82 support during construction.

83 The basic advantage of the GRS-RW system, over a conventional cantilever structure with
84 unreinforced soil backfill, is in obviating the need to provide a piled foundation to resist the
85 lateral thrust developed due to active earth pressure conditions, the large internal moments, and
86 shear forces developed in the facing. This is particularly the case when constructing over soft
87 soils and when high wall heights are considered. Removing piles reduces costs dramatically
88 and makes the structure more resilient to seismic events where large ground movements may
89 occur. The base ground for existing *in-situ* GRS-RW walls was improved by using 1m deep
90 cement-mixed soil with a cement content of 150kg per cubic meter, and above that, a drainage
91 layer consisting of crushed gravel was placed (Tatsuoka, et al., 2007). The degree of
92 compaction applied to the backfill, and the induced tensile stresses in the geosynthetic
93 reinforcement are critical elements of the construction technique to ensure a successful
94 installation, i.e. to significantly reduce lateral pressure on the facing. Pre-loaded and pre-
95 stressed gravel backfill for GRS-RWs with full-height rigid facing has also been implemented
96 in practice for a railway line in Kyushu Island, Japan. Its high seismic stability capability was
97 confirmed through model shaking tests (Koseki, 2012).

98 A strong connection between the facing and the backfill is essential for a stable GRS-RW
99 structure. The gravel-filled bags placed at the wall face have a very high drainage capacity and
100 thus any excess pore pressure generated in the backfill during loading can efficiently dissipate
101 to leave a drained condition (**Figure 1b**). Furthermore, some of the facing concrete penetrates
102 the surface zone of the gravel-filled bags during placement and therefore increases the contact
103 strength between the concrete facing and the bags.

104 In order to investigate the performance of railway track structures under static and cyclic
105 loading, full-scale laboratory testing has been used by many researchers (Čebašek, et al., 2018;
106 Woodward, et al., 2014; Bian, et al., 2014; Brown, et al., 2007; Yu, et al., 2019). With the help
107 of this useful approach, short- and long-term behaviour of railway track components have been
108 investigated. As a consequence of cumulative deformation under repeated loading, various
109 settlement models have been proposed (Alva-Hurtado & Selig, 1981; Shenton, 1985; Sato,

110 1995; Bian, et al., 2014; Selig & Waters, 1994; Thom & Oakley, 2006; Indraratna, et al., 2012).
111 Comparisons between experimental and analytical models have been performed by Dahlberg
112 (2001) and Abadi et al. (2016), highlighting two phases of settlement which consist of a non-
113 linear relationship between the number of cycles and initial settlement followed by a linear
114 trend. Čebašek et al. (2018) compared the performance of ballasted track against slab track on
115 conventional embankment. Their results demonstrated that settlement of the concrete-slab
116 track is significantly lower than that of ballasted track under similar loading and ground
117 conditions.

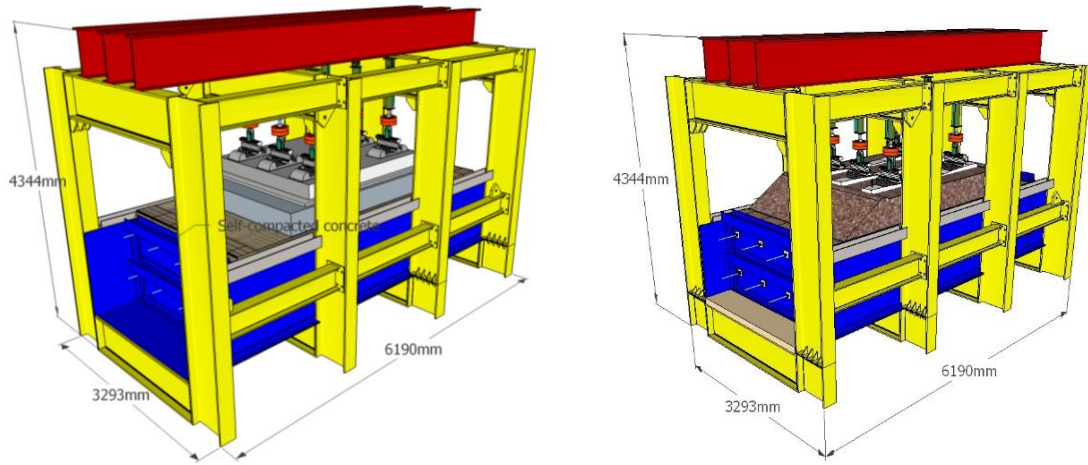
118 This research work seeks to provide a technical insight of an adoption of the GRS-RW system
119 for both developing and developed countries which are set to expand high-speed rail
120 infrastructures rapidly while increasing the track performance and reducing the construction
121 costs. In this study, the purpose is to compare a concrete-slab and ballasted tracks on GRS
122 embankment. Short and long term behaviour are investigated using a full-scale testing facility
123 called Geo-pavement and Railways Accelerated Fatigue Testing (GRAFT-2). The
124 superstructures are positioned over a geosynthetically reinforced soil with retaining wall (GRS-
125 RW) system and subjected to static and cyclic loading. The testing facility, construction of the
126 structure, track components and material parameters are all described in Section 2 of the paper.
127 The loading methodology and data acquisition are presented in Section 3 and the analysis of
128 the results are discussed in Section 4, followed by the Conclusions of the testing programme.

129 **2 Laboratory testing**

130 In this section, the methodology of the tests, experimental setup, materials and their associated
131 properties are described.

132 **2.1 Methodology**

133 A GRS-RW system was investigated in controlled laboratory conditions using GRAFT-2
134 facility (**Figure 2**), located at Heriot-Watt University. The accelerated testing approach means
135 multiple axle passages can be simulated in a short time period. This was achieved using six
136 independent hydraulic actuators loading three full-sized sleepers on a ballasted track or on a
137 concrete slab track via built-in baseplate locations on the concrete surface. This simulated the
138 passage of a moving axle (using phased loading), with each piston applying loads on a given
139 rail segment as indicated in **Figure 4**. The primary objective of testing was to assess and
140 characterise the short- and long-term settlement behaviour of a GRS-RW structure subjected
141 to cyclic loading using the two different track forms. Firstly, the concrete slab track was tested
142 followed by the ballasted track. The results presented in this paper were performed on a GRS-
143 RW system in accordance with railway infrastructure standards. A similar testing procedure
144 was followed by Čebašek et al. (2018) in earlier GRAFT-2 testing of ballasted and concrete
145 slab-track, thus allowing for comparisons to be made with non-GRS-RW support structures in
146 future work.



147

148

149

150

Figure 2: Geopavement and Railways Accelerated Testing Facility (GRAFT-2) at Heriot-Watt University, (a) slab track and (b) ballasted track resting on GRS-RW structure

151 **2.2 Experimental setup**

152 The GRAFT-2 facility was used to test sections of a precast concrete slab track, and a ballasted
 153 track with concrete sleepers. The substructure consisted of 0.1m well-compacted base layer on
 154 top of which the 1.2 m high GRS-RW was built. The substructure layers are the subgrade and
 155 frost protection layer (FPL) from bottom to top, respectively. The sand mixture was chosen
 156 from two different batches composed of 0-6mm well-graded granular limestone **Figure 9**. The
 157 sand was comprised of 80% of 0-4mm batch and 20% of 2-6mm batch. This was adopted to be
 158 consistent with the conventional embankment testing (Čebašek, et al., 2018), and also to be
 159 consistent with HS line design where the second deformation modulus (EV_2) is 120MPa. The
 160 general concept of the GRS-RW structure for the two track types tested in the GRAFT-2 facility
 161 is presented in **Figure 3**.

162 The fill consisted of geogrid reinforced layers with symmetrically embedded bolts at selected
 163 positions. Tensar RE540 is a uniaxial geogrid made of high-density polyethylene with
 164 enhanced long-term tensile strength. The properties of the geogrids used in this study are given
 165 in **Table 1**.

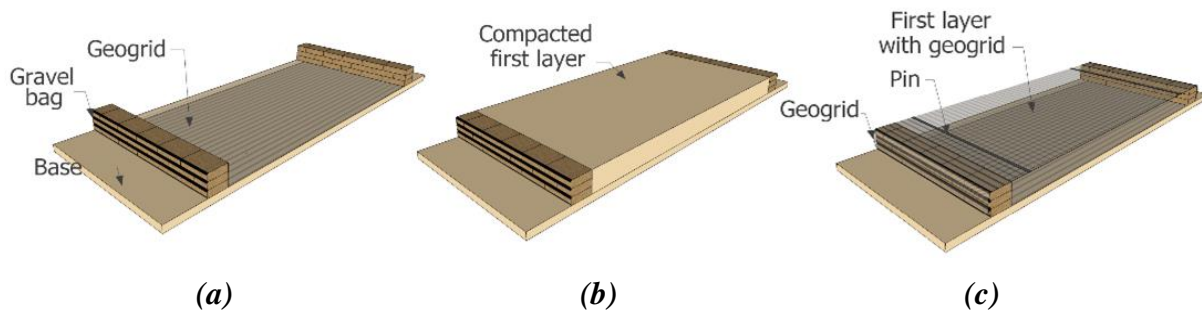
166 **Table 1:** Properties of geogrids used in soil and ballast

RE540	TX190L
--------------	---------------

Plan view

<div style="display: flex; justify-content: space-around;"> Uniaxial Triaxial </div>			
<div style="display: flex; justify-content: space-around;"> Used for soil reinforcement Used under ballast </div>			
R_L (mm)	235	Aperture shape	Triangular
R_S (mm)	16	Rib shape	Rectangular
R_W (mm)	6	Hexagon pitch (mm)	60
R_T (mm)	1.1		
B_T (mm)	2.5-2.7	Junction efficiency (%)	100
B_W (mm)	16		
Mean Aperture size	16 x 219	Mean Radial Secant Stiffness at 0.5% Strain (kN/m)	540
Short term tensile strength in longitudinal direction (kN/m)	64.5		
Junction efficiency (%)	95		

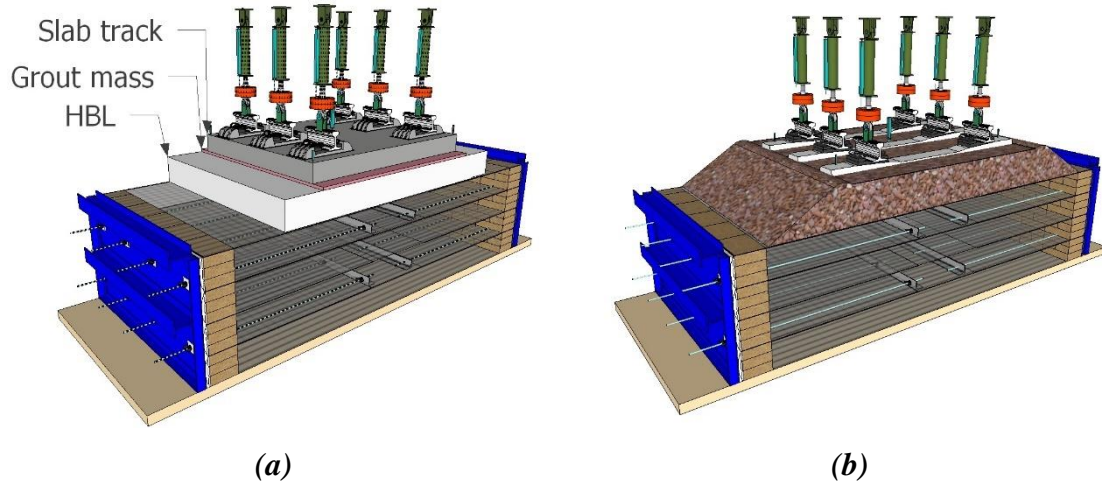
167 The geogrid was placed over the base layer then the gravel bags were positioned at the ends;
 168 the overlapping gravel bags were placed in a similar fashion to that of a brick wall construction
 169 at the shoulders (**Figure 3a**). A sand fill layer was then formed by compacting sand (**Figure**
 170 **3b**). The geogrid was then pulled and tightened over the gravel bags and pinned into the
 171 compacted soil using nails to provide tensile strength (**Figure 3c**). The geogrid was partially
 172 wrapped and hand-tightened to improve the overall stiffness of the reinforced soil. Subsequent
 173 layers were constructed sequentially up to a total wall height of 1.2m. During this construction
 174 process steel tie bars were positioned between the layers, as shown in **Figure 4** (the free-
 175 standing retaining wall is represented by the blue steel plates).



176
 177
 178 **Figure 3: The stages of the GRS-RW construction**

179 The steel tie bars were anchored within the fill subgrade by embedded steel *angle-sections*
 180 (**Figure 4a**). The steel plates were used to replicate the *in-situ* formed GRS-RW system

181 retaining wall and were only connected to the steel bars once the full subgrade structure had
 182 been formed. The gaps between the steel plate and the gravel bags were then filled with self-
 183 self-compacting concrete to form a fully connected wall retaining system.



184
 185

186 **Figure 4:** Layout of the ballast and slab tracks on GRS-RW embankment (a) concrete slab-track; (b)
 187 ballasted track

188 The gravel bags played an important role during construction as temporary (and stable) facings,
 189 resisting lateral earth pressure generated by the backfill compaction stresses and the self-weight
 190 of the structure. For the real *in-situ* structure the gravel bags facilitate the compaction of the
 191 layer during construction and create a barrier of differential horizontal and vertical
 192 displacement between the GRS structure and the wall. They also serve as a drainage route.

193 **Table 2:** CBR values of the compacted soil using Dynamic Cone Penetrometer (DCP)

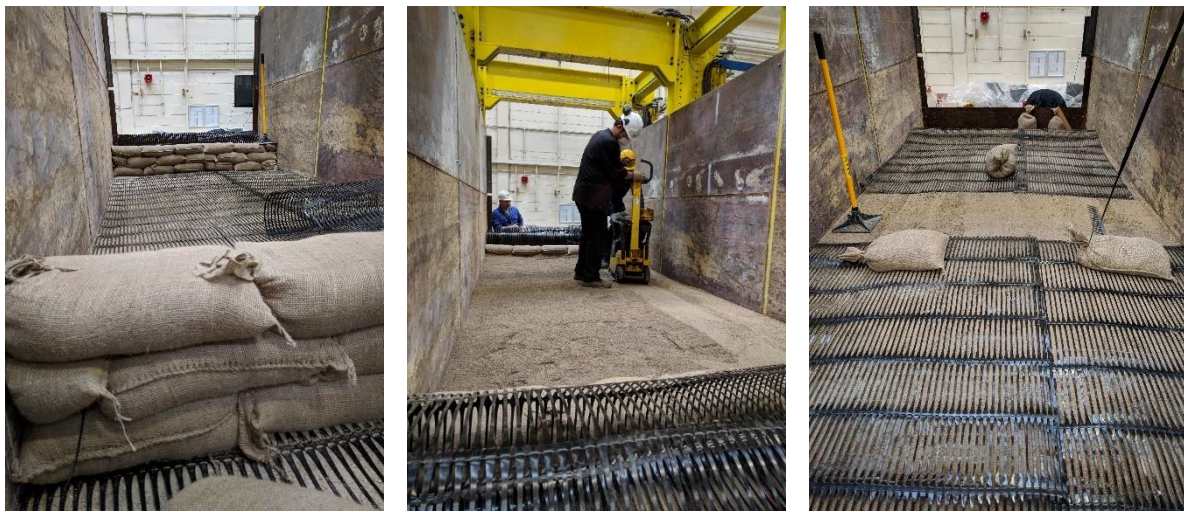
CBR Test Time	CBR value
During construction of Substructure -Subgrade	28.5
During construction of Substructure -FPL	56.1
After Removal of Slab - on top of FPL	125.1
After Removal of Ballast – on top of FPL	128.2

194 The compaction level of each 0.3m high layer was set based on a correlation with CBR values,
 195 which were obtained via measured Dynamic Cone Penetrometer (DCP) tests as shown in **Table**
 196 **2**. The correct compaction level was essential in order to achieve the required stiffness. The
 197 indicated CBR values have been identified in conjunction with the work carried out by
 198 Čebašek, et al. (2018) who made a correlation between the EV_2 and CBR.

199 2.2.1 Laboratory construction of substructure

200 Photographs of the construction stages of the substructure are highlighted in **Figure 5** and
 201 **Figure 6**. The geogrid was cut 11m long and placed on each base layer. The substructure test
 202 bed width was 5m. To cover the 2.2m width of the test bed the geogrids were placed as 2 pieces

203 of 1.2m and 1.0m widths. They were placed in such a way that at each layer the connections of
204 two pieces of geogrid did not overlap each other. The joint was staggered as the geogrid layers
205 were placed during the GRS construction. Three layers of sandbags were placed at opposite
206 ends of the test bed (5m apart) and compacted using hand tools (**Figure 5a**). Then the well-
207 graded sand was placed between sand bag walls and compacted with a forward/reverse plate
208 compactor (**Figure 5b**). The initial loose sand thickness was 200mm which reduced to 150mm
209 after compaction. The two compacted layers formed a 300mm thick total compacted layer
210 which had the same thickness as the compacted sand bag walls. The sand level was checked
211 using a conventional spirit level. Once the sand bag walls and compacted sand reached the
212 same height, the geogrid was wrapped around the bags and laid on the compacted sand (**Figure**
213 **5c**).



214

215

(a)

(b)

(c)

216 **Figure 5:** Construction stages of the GRS structure: (a) Positioning the sandbags on the geogrid; (b)
217 compaction of the sand; and (c) wrapping the geogrid around the sandbags and pinned into
218 compacted soil

219 The geogrid then was hand-tightened and fixed to the soil using nails. Each layer of reinforced
220 soil was formed following the same soil compaction parameters given in Cebasek et al. (2018).
221 The first 800mm of the subgrade was compacted to achieve an EV_2 value of 60MPa and the
222 remaining upper FPL 400mm was compacted to achieve an EV_2 value of 120MPa. As
223 commented above these elasticity values were calibrated via DCP measurements during each
224 compaction layer formation.



225

226

(a)

(b)

(c)

227 **Figure 6:** Construction stages of the GRS structure: (a) Tie bars through the sandbags and FHR wall,
 228 and anchored with angle irons; (b) Self-standing GRS soil and the cast-in HBL layer of slab track (c)
 229 FHR retaining wall positioned with topflow

230 At 300mm and 900mm depths tie bars were anchored to angle irons that were positioned half
 231 a metre from each other, i.e. in the middle of the 5m track width (**Figure 6a**). The vertical and
 232 horizontal distance of each adjacent tie bar was 600mm, which are designed according to
 233 Tatsuoka, et al. (1997). In total four layers of reinforced soil were constructed. On top of this
 234 substructure, the hydraulically bonded layer (HBL) was placed (**Figure 6b**).

235 Finally, the 0.08m gap between the GRS wall and RW was filled with ‘topflow’ as seen in
 236 **Figure 6c**. It was a ready-mix highly fluid self-compacting concrete consisting of maximum
 237 10mm diameter aggregates. This material was chosen specifically because of its ability to fill
 238 the gaps between the geogrid and sandbags through geogrid apertures. This was to provide
 239 reinforcement and resilience to the GRS. The density, Young’s modulus, and Poisson’s ratio
 240 of the topflow were determined using compression tests on cylindrical samples and found to
 241 be 2428,7kg/m³, 21.2GPa and 0.159, respectively.

242 2.2.2 Concrete slab track

243 The first form of the superstructure was constructed using a Max Bögl slab track which consists
 244 of a prefabricated reinforced concrete slab made of c45/55 concrete with characteristic cube
 245 compressive strength of 45 MPa, which is a high strength concrete. As shown in **Figure 7a**, a
 246 three-sleeper section was used for the concrete slab-track which was placed above the
 247 Hydraulically Bonded Layer (HBL). The HBL itself was of thickness 300 mm and it was made
 248 of c10/12 concrete with characteristic cube compressive strength of 10 MPa, which is a
 249 lightweight and low strength concrete. After 21 days, the slab was positioned above the HBL
 250 supported by hard wooden wedges. Then ‘Conbextra HF’, a high-flow, non-shrink,
 251 cementitious grout, for grouting gap thicknesses between 10 to 100mm, was used between the
 252 slab and the HBL.



253

254

Figure 7: Slab track in the GRAFT-2 testing facility

255 The rail fastening system was the 300-1 Vossloh Fastening System. From bottom to top the
256 rail support consisted of three layers: an EPDM pad, which is a soft synthetic rubber railpad, a
257 steel baseplate, and an EVA, which is a stiff copolymer pad for rail seating, respectively. The
258 static stiffness of the EPDM was about 22.5kN/mm and the dynamic stiffness was about
259 40kN/mm. The static stiffness of the EVA pad was about 600–700kN/mm and the dynamic
260 stiffness was about 1600–1800kN/mm. The cut rail segments used in the slab track test were
261 60E1 (UIC 60).

262 **2.2.3 Ballasted track**

263 After completion of the slab track tests, the superstructure including the HBL, grout and
264 concrete slab were removed from the facility. The surface of the substructure soil required
265 removal as the HBL layer disturbed the upper soil layer. The upper 50mm of sand was therefore
266 excavated and replaced with a new sand layer which was then compacted to achieve the same
267 stiffness as the subgrade prior to the concrete slab track test. A triangle-aperture geogrid
268 TX190L was placed on top of the substructure to provide additional support to the ballast.
269 **Figure 8** shows the position of the sleepers (standard G44s) on the ballast bed at a typical
270 industry spacing of 650mm. The ballast bed was placed and compacted in four equal layers of
271 100mm intervals and hence its overall thickness underneath the sleepers was 400mm. In order
272 to reach the required ballast compaction, an electric compactor with a 400mm by 320mm
273 vibrating plate was used to compact each 100mm thickness ballasted layer. As a result, the bulk
274 density of the compacted ballast was approximately 16kN/m³.



275

276

Figure 8: Ballast track in the GRAFT-2 testing facility

277

278

279

280

281

282

283

284

285

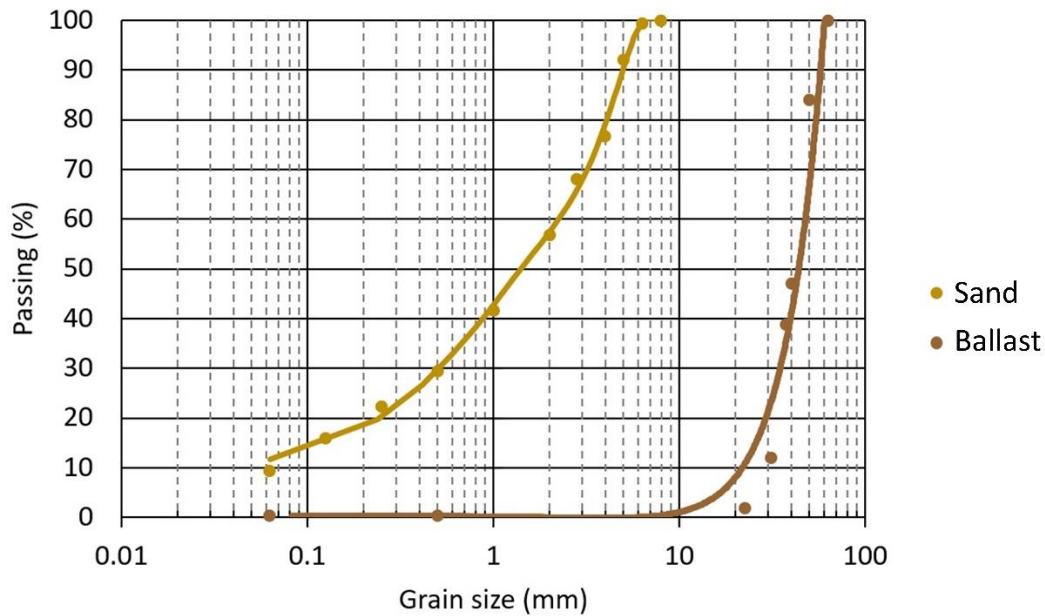
286

287

288

289

The ballast aggregate was composed of micro-granite at 0.5% moisture content. The plot of **Figure 9** indicates the gradation curve of the ballast which is a good match for a typical railtrack ballast curve, compared to that of the sand curve used to construct the subgrade and FPL. The lower EPDM elastic pads used in the ballast test were the same rail pads as those used in the concrete slab track test. Pandrol's fast clip fastening system was used to restrain the loaded rail segments to the sleepers. Sections of BS113A (56E1) rail segments were used in the ballasted track test. The purpose of the rail segments use was to allow the connection of the actuators to the sleepers. As these were separate rail segments, they did not contribute to the bending stiffness of the track in the experiments and thus they did not have any effect on the track deformation. The rail segments' role is to be the connectors between the track and the actuators. *Note: this is often normal practice in the laboratory testing of railway track.* More than 3 million load cycles were applied in this ballasted-track test following the same procedure as that applied in the concrete slab track tests.



290

291

Figure 9: Sieve analysis for sand and ballast.

292 Specimen preparation and excavation in the full-scale testing facility required the largest
 293 amount of time and energy during this study. Overhead cranes and forklifts were employed
 294 while handling the 1t bags, sleepers, slabs and other heavy tools. A bobcat excavator and trucks
 295 were used during the excavation process. While levelling the slab was easy, as the layer
 296 underneath the slab was a highly fluid cementitious mixture, the sleepers in the ballast tests
 297 were hard to level due to uneven surface of ballast and this eventually led to some tilt during
 298 the testing, whereas in the field the continuous rails help to prevent this rotational movement,
 299 although a degree of ballast voiding may still occur.

300 **3 Testing procedure and data acquisition**

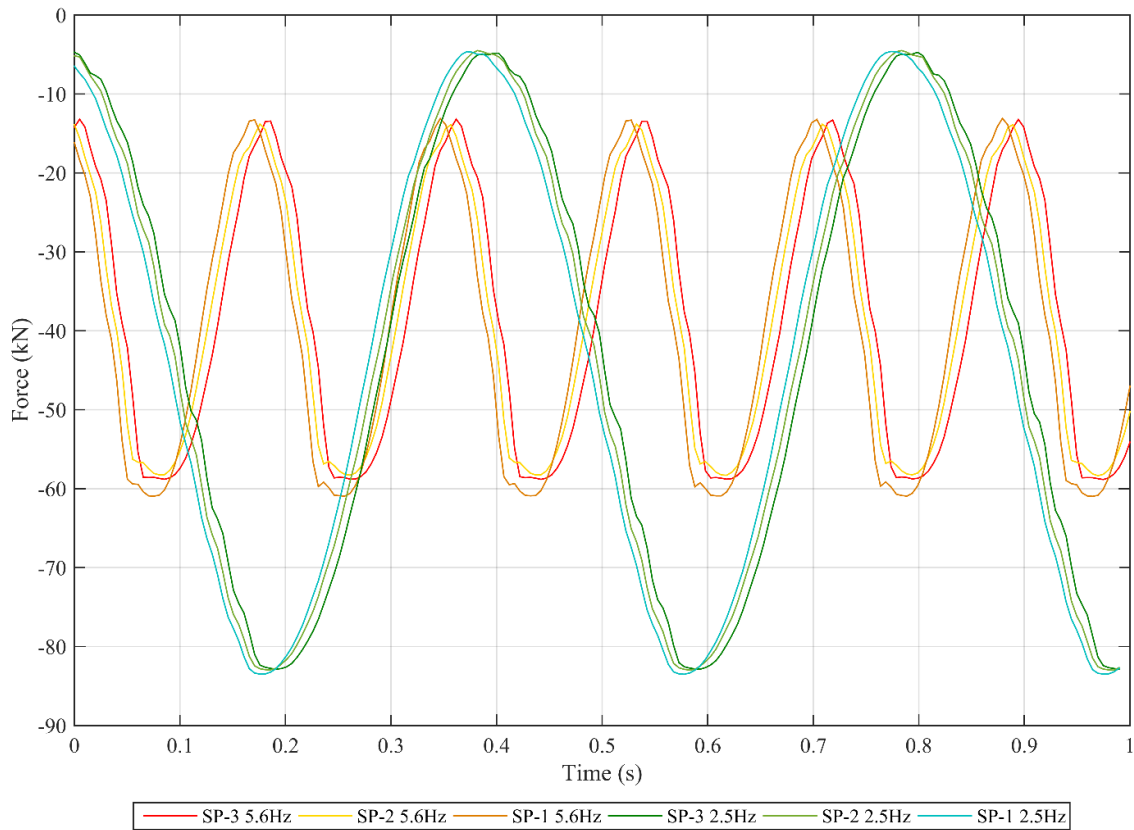
301 The same load combinations and durations were implemented in the tests presented in this
 302 paper as those used in the experiments carried out by Čebašek et al (2018); this is to allow the
 303 reader to directly compare between substructure types. As described by Čebašek et al (2018),
 304 redistribution of the axle load was applied over the three-sleeper sections for the static loading
 305 case. While half of the axle load was applied on the middle sleeper, one quarter axle load was
 306 applied on each neighbouring sleeper. In this way, 100% of the axle load is distributed over the
 307 three-sleeper track section during static loading. This approximate redistribution approach was
 308 derived from beam-on-elastic-foundation (BOEF) theory. This approach to track deflection
 309 analysis replaces the individual sleepers with a continuous support where the load is
 310 proportional to the vertical displacement (Powrie, 2016; Connolly, et al., 2020). Young's
 311 modulus and 2nd moment of area of rail, and track stiffness are the main parameters considered
 312 for the redistribution. The load redistribution, caused by an axle resting on a 3-sleeper section
 313 with continuous rail, was implemented using a static loading method (Bian, et al., 2020). For
 314 the dynamic loading case, however, each axle load was applied on each sleeper separately
 315 without any redistribution. This approach was implemented to both simulate a worst-case
 316 scenario and to allow direct comparisons of settlement behaviour between different track types
 317 and substructure forms for the same cyclic loading condition. This decision was considered an

318 important aspect of these particular tests, i.e. to provide a baseline by which performance
 319 comparisons could be made and hence future computer models calibrated. In essence, an
 320 attempt has been made to standardise the testing programme. **Table 3** shows the details of each
 321 considered loading case.

322 **Table 3:** Loading sequences of the ballasted and concrete slab track tests.

TEST	Axle load on middle sleeper (kN)	Redistribution of load per actuator (kN)	Redistribution of the load over the sleeper (%)	Frequency (Hz)	Time interval between sleepers (s)	Duration
Static I	63.77	15.94, 31.88, 15.94	25, 50, 25	N/A	N/A	600 s
Static II	83.38	20.84, 41.69, 20.84	25, 50, 25	N/A	N/A	600 s
Dynamic I	117.72	58.86, 58.86, 58.86	100, 100, 100	5.6	0.0065	1.17x10 ⁶ cycles
Dynamic II	166.76	83.38, 83.38, 83.38	100, 100, 100	2.5	0.0065	2.20x10 ⁶ cycles

323 Two static tests and two cyclic tests were performed. In the static tests, first, a 13-tonne axle
 324 load with redistribution was applied on the track for approximately 10 minutes and then the
 325 load was increased to simulate a 17-tonne axle load for the same length of time. After these
 326 initial tests, cyclic loading began without any load redistribution, by applying a 17-tonne axle
 327 load on each sleeper with a time phase lag. The sleepers were therefore subjected to repeated
 328 loads to simulate moving axles at 360km/h at a set distance (frequency). Lekarp, et al., (2000)
 329 illustrated an element subjected to stress pulses due to a moving wheel load. The vertical and
 330 horizontal stress are positive in the soil throughout the passage of the wheel, whereas the shear
 331 stress is reversed while the loading is passing by and causing a rotation of the principal stress
 332 axes. The principal stress rotation significantly affects the permanent settlement. It is noted that
 333 the stationary cyclic loading cannot fully reflect the stress rotation pattern (Bian, et al., 2020).
 334 The phased nature of the loading allows for principal stress rotation effects to be
 335 simulated. **Figure 10** shows a typical phase/time lag between the sleepers; this phasing mimics
 336 the axle moving from one sleeper to the adjacent one in 0.0065 seconds. The cyclic tests were
 337 performed at 2 different frequencies: 1.17 million cycles at 5.6Hz and 2.2 million cycles at
 338 2.5Hz. The load applied at 5.6Hz was 58.86kN per actuator, giving 117.72kN per sleeper, and
 339 the load at 2.5Hz was 83.38kN per actuator, giving 166.76kN on each sleeper (**Figure 10**).



340

341

Figure 10: Time interval of sequential loading of different frequencies in a second

342

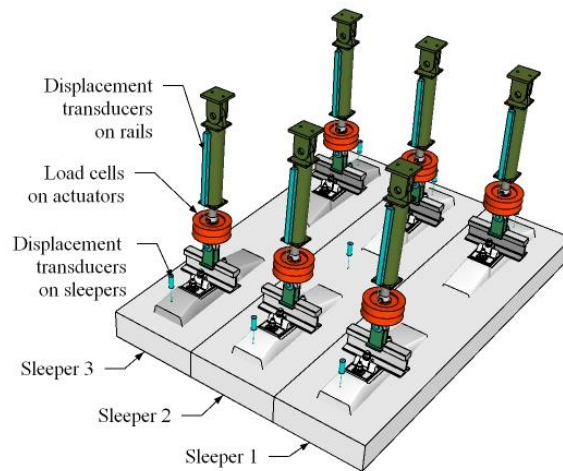
343

344

345

346

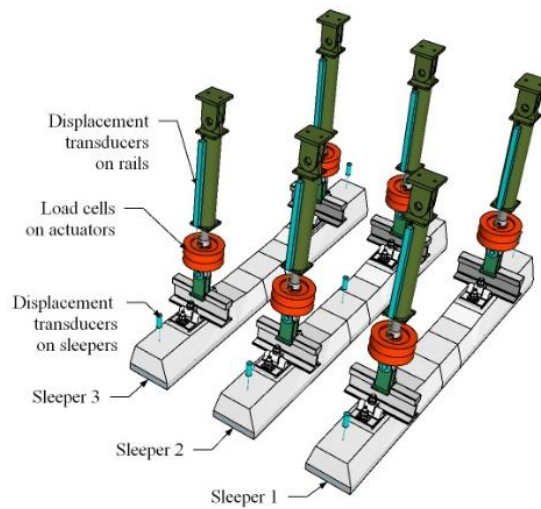
There were 32 channels actively used to acquire data. The sampling rate of the data acquisition system was 200Hz per channel and each individual item of measuring equipment was connected to a separate channel. Due to the volume of data collected, this paper concentrates on those measurements from the displacement and load cells transducers only. To control the stroke of the actuators, six 300mm long displacement transducers (LVDT) were used.



347

348

(a)



(b)

Figure 11: LVDT positions and labels (a) slab track (b) ballasted track

349

350

351

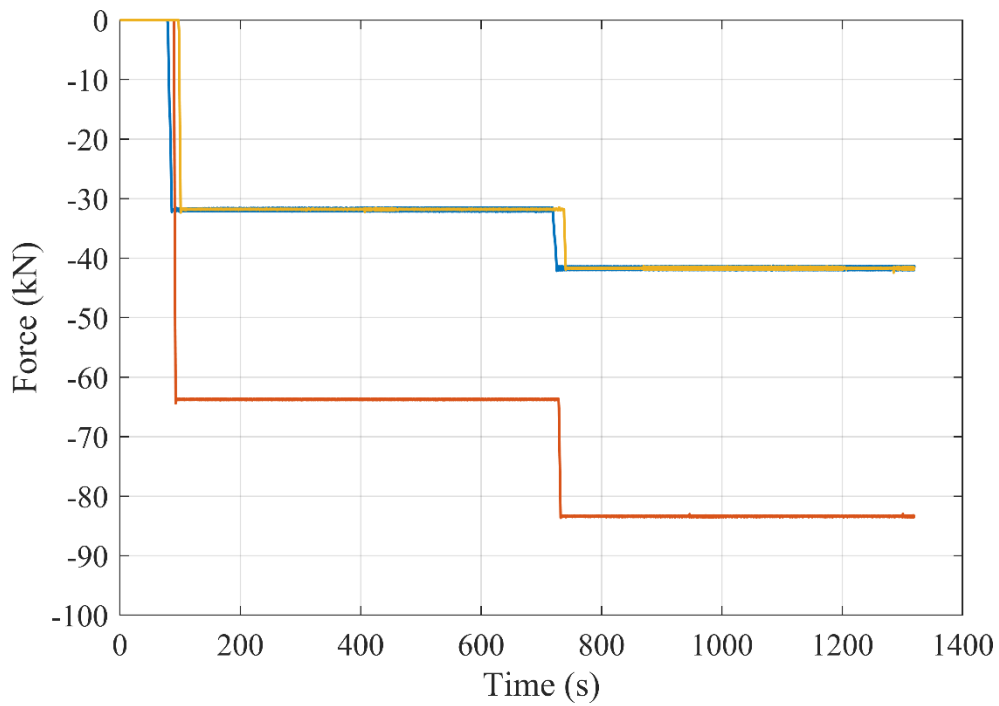
352 The displacement transducers' locations are represented in **Figure 11**. The LVDT choice was
 353 crucial for these tests as both the instantaneous/transient displacement under one cycle, and
 354 settlement, which is the permanent deformation under millions of cycles, must be plotted with
 355 the same LVDT acquired data. Therefore, they both needed to be sensitive enough to record
 356 the sinusoidal motion of the slab, which acquired a hundredth of a millimetre, as well as the
 357 accumulated settlement of the sleepers in the ballast after 3.4 million cycles, which was greater
 358 than 10 millimetres. The positioning of the LVDTs on the track was set to investigate the elastic
 359 deformation of the track as well as the total settlement under accumulated cycles.

360 **4 Analysis**

361 In this section, results related to the static and cyclic tests are presented and analysed.

362 **4.1 Static compressive loading**

363 As mentioned earlier, an initial static distributed axle load was applied on the two tracks. Firstly,
 364 13t (127.54kN) and then 17t (166.76kN) were applied for a duration of approximately 10
 365 minutes each (**Figure 12**). The distribution of these axle loads, over the three-sleeper area, is
 366 described in **Table 3**.



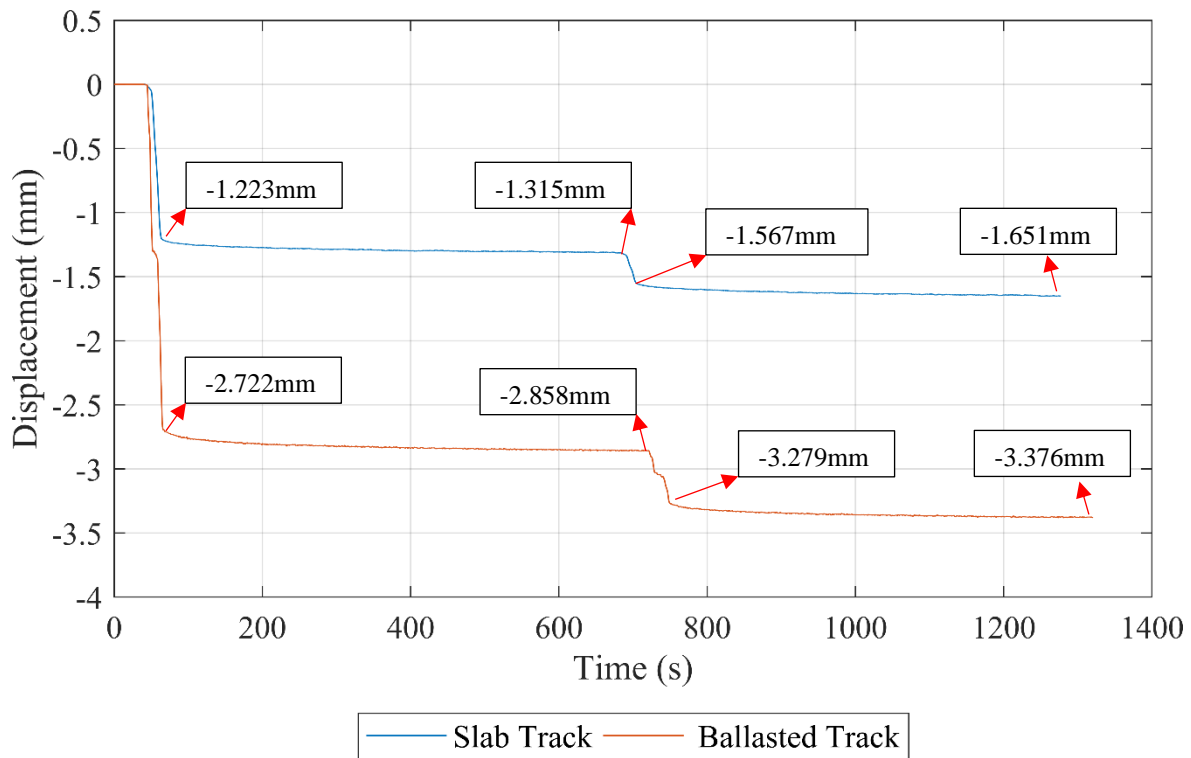
— Sleeper 1
 — Sleeper 2
 — Sleeper 3

367

368

Figure 12: Distribution of axle loads over three sleepers

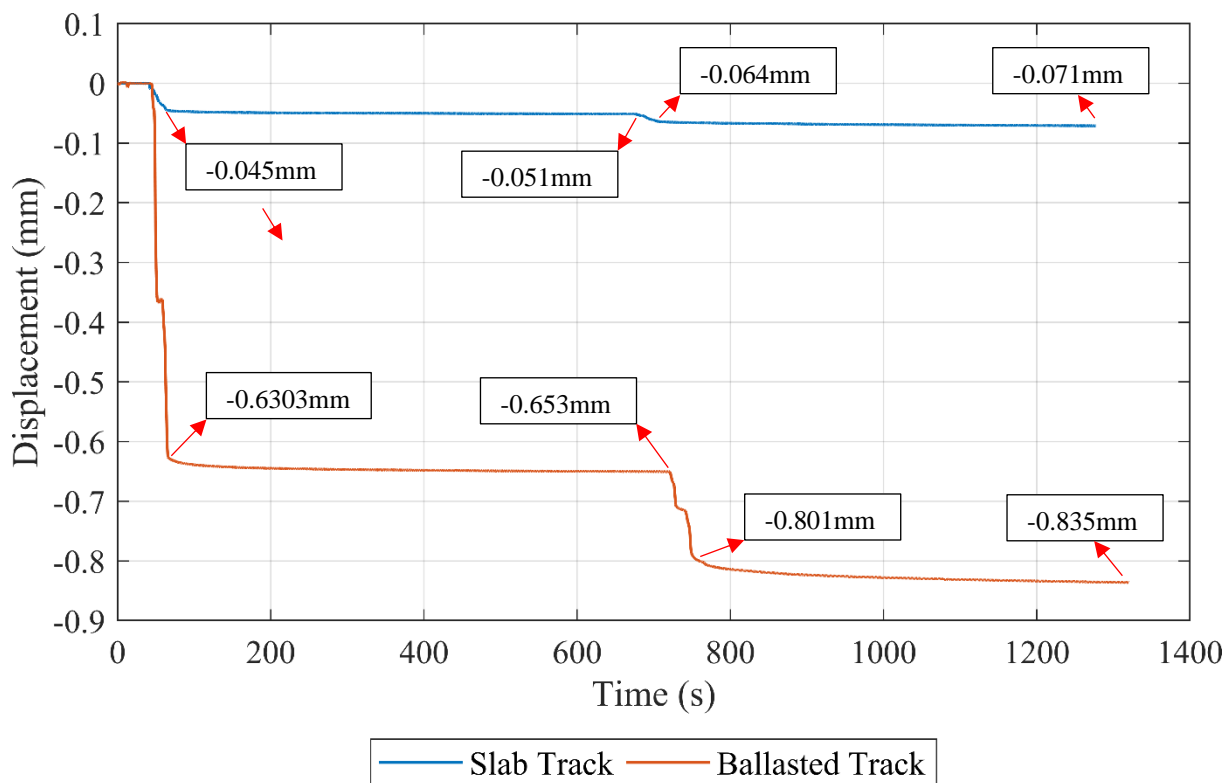
369 The red line in **Figure 12** represents half of the axle load applied on the middle sleeper (Sleeper
 370 2) while yellow and blue lines represent the quarter of the axle load applied on the adjacent
 371 sleepers (Sleeper 1 and Sleeper 3). After completing the static tests, the load was taken off.
 372 Since the displacement transducers on the rails and the sleepers show similar results, the
 373 average reading of the transducers was used for the analysis. For example, while analysing the
 374 displacement of the sleepers, the corner LVDTs (Sleepers 1 and 3) were considered. The
 375 average of the relative readings of the transducers at certain times was calculated.



376

377 **Figure 13:** Average vertical displacement of the rails for concrete slab track and sleepers on ballasted
 378 track under static loading

379 As can be seen in **Figure 13**, the average displacements of the rails of the slab track are nearly
 380 half of those on the ballasted track. The displacement of four rail segments, on the sleepers 1
 381 and 3, was taken into account. It is evident that under the static loading, a large part of the rail
 382 displacement is caused by the ballast bed because the same rail pads were used for both types
 383 of tracks. The displacement under stationary loading indicates a similar value of rail
 384 displacement for ballasted and slab track over the two 10-minute-long loading period, which is
 385 around 0.1mm. However, during the static loading when the load increased from 0 to 13t and
 386 then from 13t to 17t, the displacement of the rail on ballasted track was nearly double.



387

388 **Figure 14:** Vertical displacement of the track on the corners for concrete slab track and sleepers on
 389 ballasted track

390 **Figure 14** shows the displacements on the corners of the concrete slab-track and the ballasted
 391 track (Sleeper 1 and Sleeper 3). As expected, the displacements of the sleepers on ballasted
 392 track are higher due to the unbound and less stiff nature of the ballast. These displacement
 393 values were obtained from the four LVDTs positioned on the surface of the sleepers 1 and 3.
 394 The vertical displacement of the ballasted track was more than 10 times the displacement of
 395 the slab track when the load was increased from 0 to 13t and then from 13t to 17t. The
 396 displacement of the sleepers in the ballasted track during the stationary load was nearly 4 times
 397 larger compared to that of the slab track. These results highlight the superior load-distributing
 398 properties of the concrete slab-track and hence the reduction of the stress concentrations on the
 399 GRS trackbed. The total plastic settlement of the ballasted track after releasing the load was
 400 0.331mm, whereas the slab only settled 0.019mm.

401 A notable result from the static compression load tests on the concrete slab track was the
 402 improved performance of the GRS structure when compared to the ballasted track. In addition
 403 to the weight of the HBL, concrete slab and rail segments, 13 tonnes and 17 tonnes of load
 404 were applied, and thus, the GRS structure endured firmly. Moreover, the vertical displacement
 405 after about 20 minutes of static loading was only 0.07 mm and the total plastic settlement was
 406 0.019mm after removing the load.

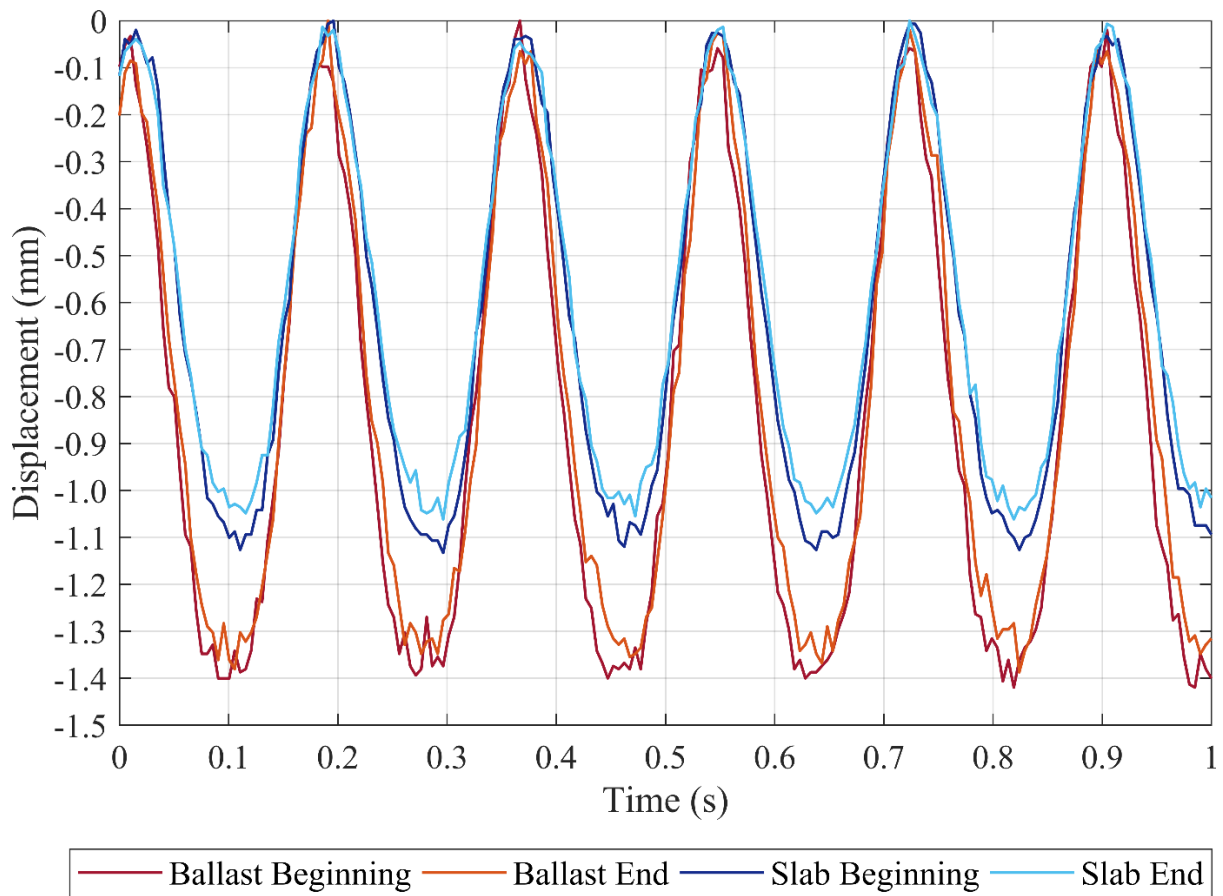
407 4.2 Cyclic loading

408 In a stable track structure, the magnitude of the axle loads and their accumulation (load cycles)
 409 are the main reasons for the permanent vertical track settlement. This plastic settlement, due to
 410 *the track tonnage*, leads to changes in the track geometry and hence a deteriorating ride quality.

411 The transient displacement under individual axles is an important component of the track
412 behaviour. For example, in a ballasted track, if the track stiffness is too low then increased
413 settlement will likely occur, if it is too high then increased rail wear may result. Each layer's
414 individual elastic stiffness modulus contributes to the transient displacement. In conventional
415 ballasted track, vertical stresses reduce relatively quickly with depth compared to the trackbed
416 displacements. In addition to the elastic stiffness modulus of the individual trackbed layers
417 below the ballast, the unbound nature of the ballast itself is another reason for higher
418 displacements of ballasted tracks when compared to a bound system, such as concrete slab
419 track. This is because the elastic stiffness modulus of the unbound ballast is a function of its
420 effective confining pressure as well as other properties such as aggregate angularity and
421 density.

422 The key parameters leading to the observed settlements and vertical displacements were
423 identified via analysing both total and individual cycles. The cycles were chosen at the
424 beginning and at the end of the tests to determine the stiffness change in the track under high
425 levels of cyclic loading (tonnage). In general, vertical displacement data is represented per
426 second and for two different frequencies of 5.6Hz and 2.5 Hz. The total settlement is also
427 plotted for both frequencies for 1.2 million and 2.2 million cycles, respectively. These points
428 have been chosen so that comparisons to the Čebašek et al. (2018) paper can be directly made.

429 The mean magnitude of the rail and the sleeper displacements were calculated based on the
430 four LVDTs placed at the sleepers 1 and 3, and in the corners of the slab track. The smoothness
431 of the cycles is directly related to the performance of the data acquisition system; it was found
432 that the LVDTs on the slab and sleepers were more sensitive than the ones on the rails.



433

434

435

Figure 15: Average displacement amplitudes of the rails on ballast and concrete slab track at the beginning and the end of the 5.6Hz cycling at 13kN to 58.9kN

436

437

438

439

440

The amplitudes are taken 1000 cycles from the beginning of the tests and 1000 cycles before the end. The average displacement of the rails on the slab at 5.6Hz loading was 1.1mm, whereas it was 1.4mm in the case of the ballasted track (**Figure 15**). The magnitude of the load at this frequency was oscillating between 13kN and 58.9kN. The reduction in the amplitude of the rail displacement was 0.05mm for both tracks.

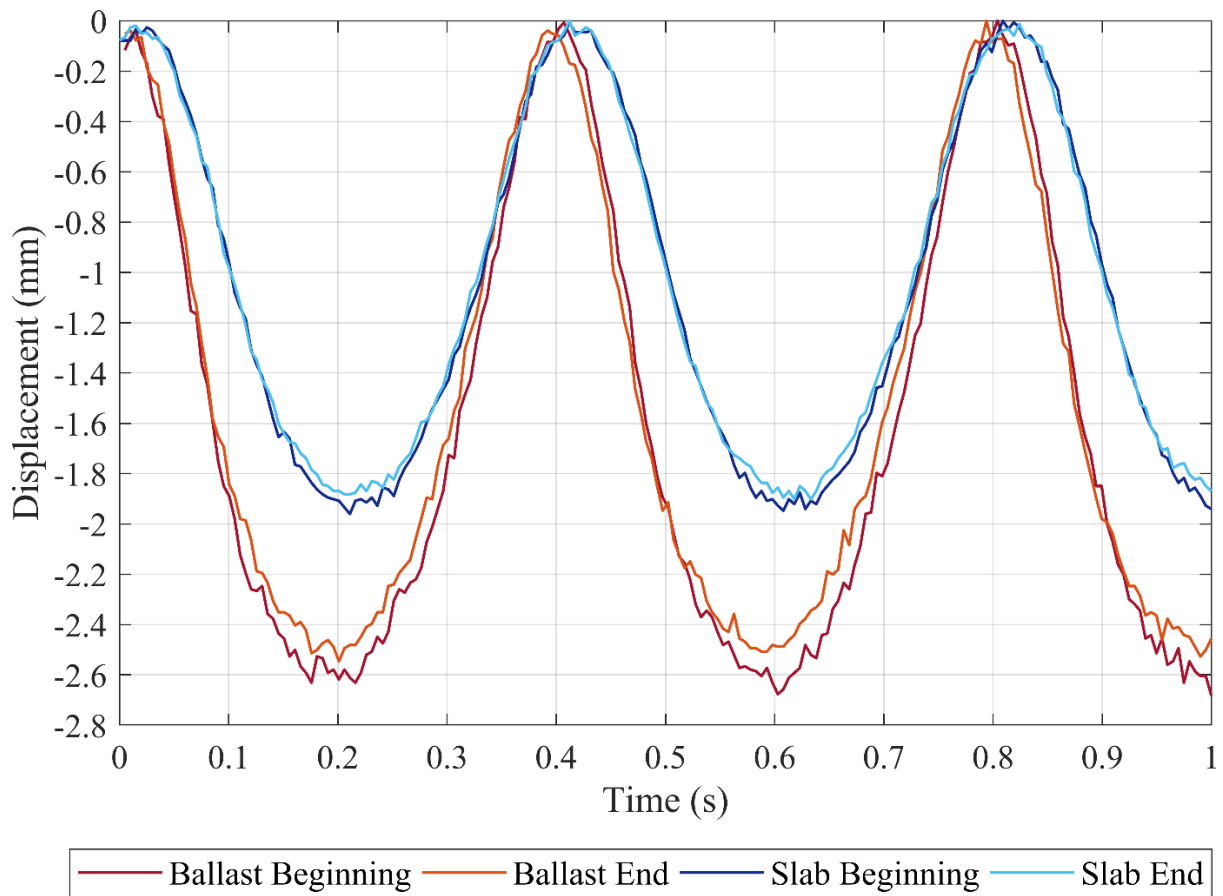


Figure 16: Average displacement amplitudes of the rails on ballast and concrete slab track at the beginning and the end of the 2.5Hz cycling at 5kN and 83.4kN

In **Figure 16** the mean displacements of the rails on both tracks are presented. The rail on the slab deflected around 1.9mm, whereas in the ballasted track case it deflected 2.6mm under 83.4kN cyclic loading (as mentioned above this equates to a phased 17t axle load on individual sleepers without redistribution). The reduction in amplitude in the slab's rail displacement was much smaller than that on the ballasted track.

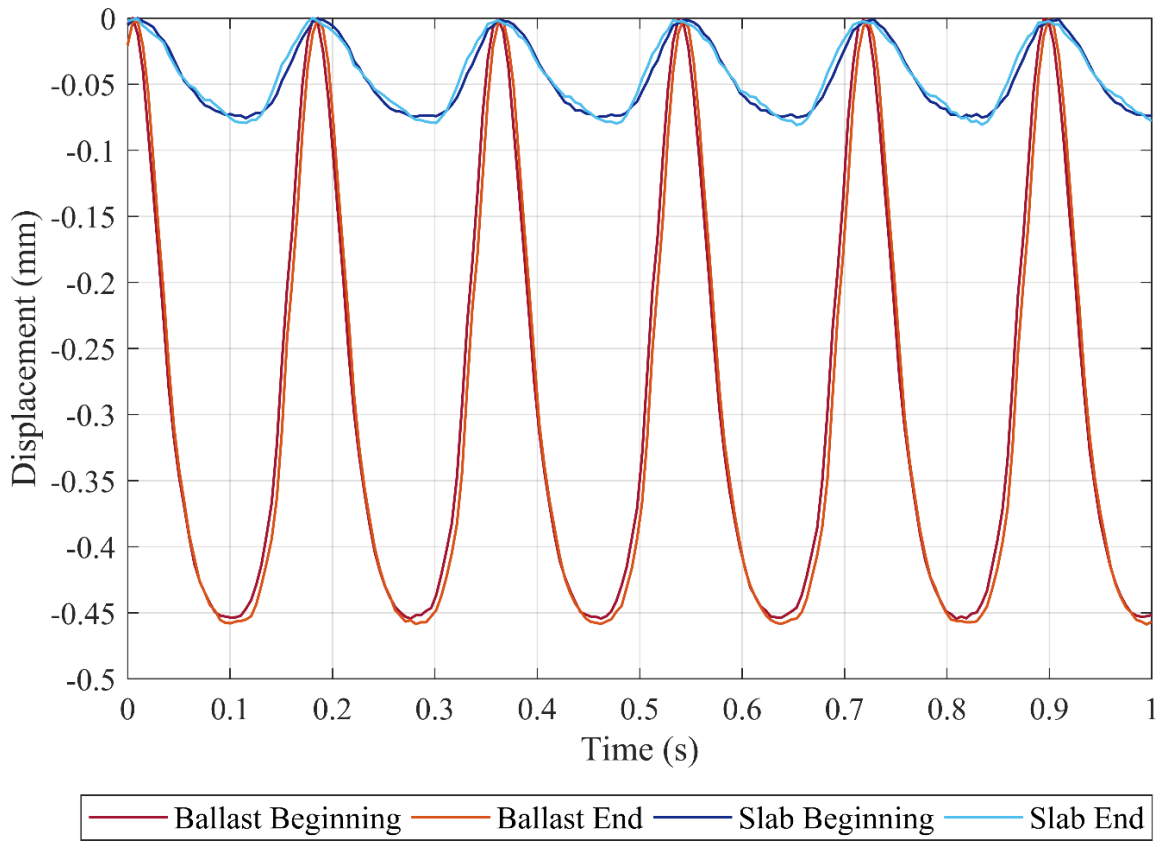


Figure 17: Average displacement amplitudes of the sleepers of ballast and concrete slab track at the beginning and the end of the 5.6Hz cycling at 13kN to 58.9kN

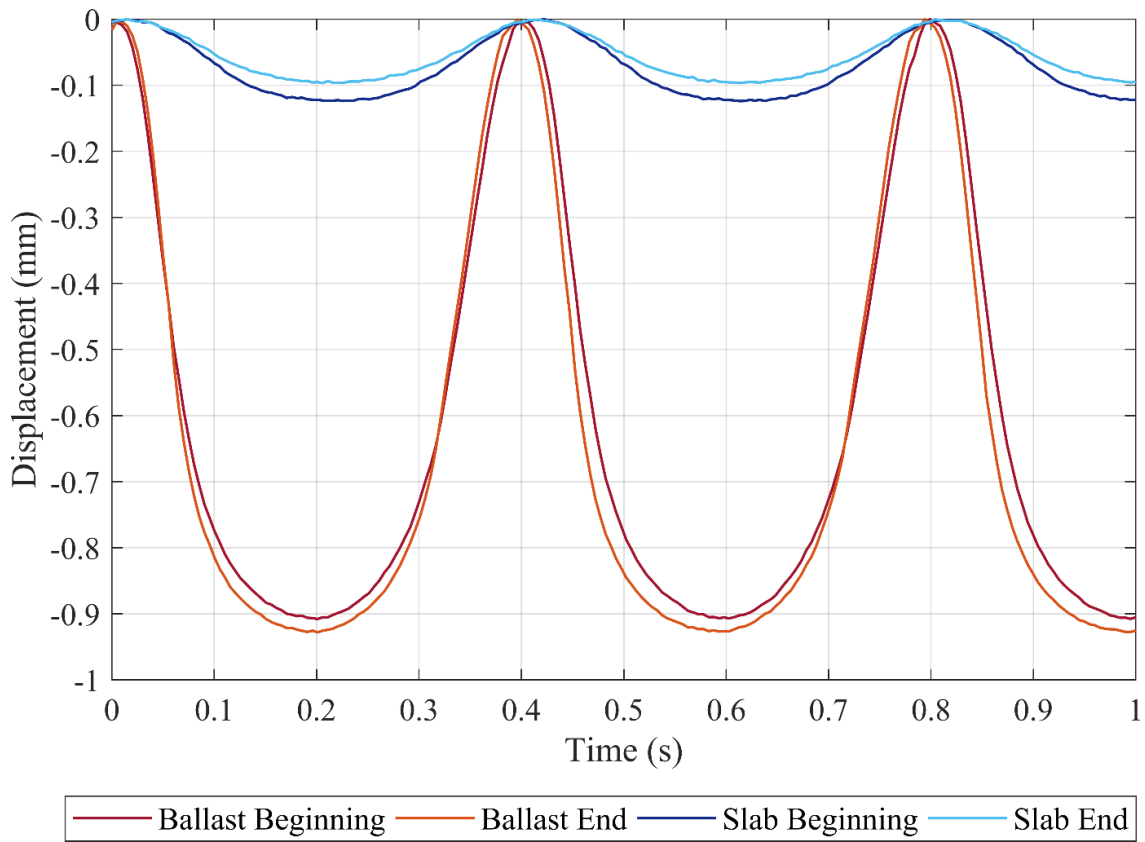


Figure 18: Average displacement amplitudes of the sleepers of ballast and concrete slab track at the beginning and the end of the 2.5Hz cycling at 5kN and 83.4kN

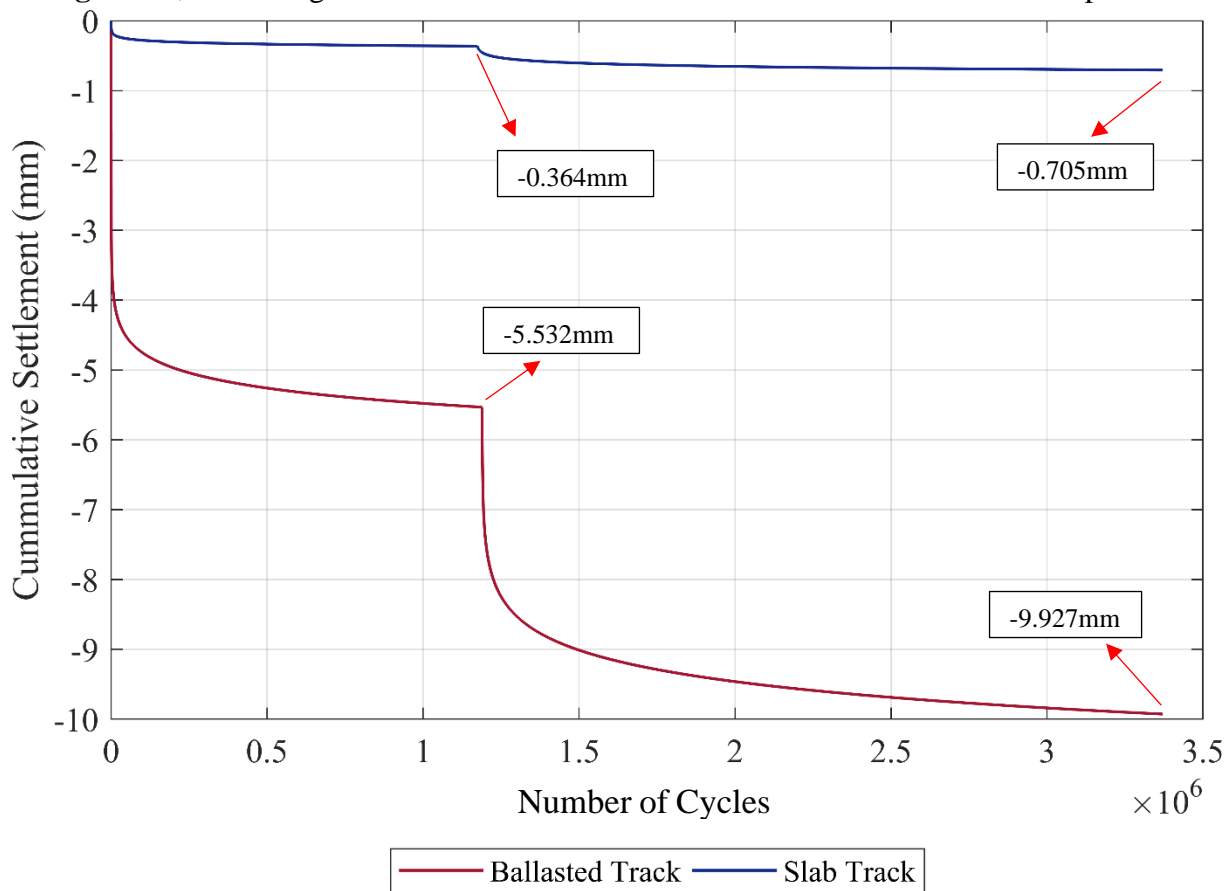
455 **Figure 17** and **Figure 18** indicate the mean displacements of the sleepers in the ballasted track
456 and the slab under 5.6Hz and 2.5Hz loading. Contrary to the elastic behaviour of the slab, ballast
457 performed in a more complex manner due to its unbound and non-linear nature. While
458 the transient displacement of the slab was quite uniform according to the LVDTs on the slab,
459 the displacement of the sleepers in the ballast varies significantly among the LVDTs. The
460 average overall displacement of the LVDTs at the end of each loading phase was slightly greater
461 than the average overall displacement of the LVDTs at the start of the loading. This was traced
462 to one LVDT which exhibited a slight inconsistency in readings between the beginning and
463 final displacements for the ballasted track. This LVDT recorded a 0.13mm increase in
464 displacement over 2.2 million load cycles, whereas all the other LVDTs generally showed a
465 slight reduction in the amplitude (as would be expected). This increase in displacement is,
466 however, very small (a fraction of a mm) compared to the full amplitude of each sleeper
467 displacement. It is conceivable that this may indicate a small movement of the anchoring system
468 near this particular LVDT, but could also simply be within experimental error of the
469 measurement system for this particular LVDT over the 2.2 million load cycles. Even so, the
470 average of the LVDTs was presented for the consistency in the representation. These LVDTs
471 were placed on the surface of the slab and the sleepers.

472 The mean displacement of the slab under a single cycle at 5.6Hz loading was 0.079mm and
473 0.111mm at 2.5Hz, which corresponded to load increase from 58.9kN to 83.4kN, respectively.
474 The displacement of the sleepers in the ballasted track was 0.45mm throughout the 5.6Hz
475 loading. It was 0.9mm when the frequency decreased to 2.5Hz because the load increased from
476 58.9kN to 83.4kN, as mentioned above.

477 Overall, the rail displacement is directly linked to the displacement of the wheels and is always
478 higher than the sleeper displacement due to the presence of the railpads. The displacements of
479 both rail and sleeper are recorded during the testing for future analysis of the railpads efficiency
480 in reducing the transmitted displacement.

481 **4.3 Permanent Settlement**

482 In **Figure 19**, the average cumulative settlement of the slab and ballasted tracks are presented.



483

484 **Figure 19:** Cumulative settlement of slab and ballasted track at each frequency vs the number of
 485 cycles

486 The blue curve shows the settlement values at the corners of the concrete slab track. The average
 487 cumulative settlement of the concrete slab track is 0.705mm under two consecutive stages of
 488 cyclic loading. The average settlement for the first loading phase (5.6 Hz for 1.2 million cycles)
 489 is 0.364mm, whereas the rest of the cumulative settlement is generated by the second phase of
 490 loading (2.5Hz for 2.2 million cycles). The red curve shows the settlement values at the end of
 491 the sleepers 1 and 3 in the ballasted track. The average cumulative settlement at 5.6Hz for 1.2
 492 million cycles was 5.532mm, whereas the rest of the cumulative settlement is generated by the
 493 second phase of loading (2.5Hz for 2.2 million cycles) and reaches 9.927mm.

494 As with other track tests reported in the literature, significant parts of the plastic deformation
 495 are generated by the initial load cycles. After this initial phase, the settlement follows a reduced
 496 downward trend in the ballasted track. In the concrete slab track tests, the track shows a much-
 497 reduced settlement curve after the initial cycles compared to that of the ballasted track (i.e. it
 498 starts to level off very quickly).

499 **5 Conclusion**

500 A geosynthetically reinforced soil with retaining wall (GRS-RW) was tested at full-scale as an
 501 alternative to a conventional rail embankment. The soil fill (subgrade) was formed of two layers

502 at different stiffnesses and were compacted to high-speed rail standards. The soil stiffness
503 parameters were measured using *in-situ* soil testing techniques and the soil was reinforced using
504 uniaxial geogrids wrapped around granular bags. These bags provide lateral confinement during
505 placement and compaction of the fill materials.

506 A three-sleeper section of a concrete slab track and a ballasted track were placed on the GRS
507 structure alternately. The loads were applied using six individual actuators connected to the
508 track superstructure via a rail connector. Firstly, two different static loads were applied with
509 redistribution over the track structure to account for the bending stiffness of a rail section. Then
510 two different cyclic loading frequencies were applied in a phased manner to mimic a train
511 moving at 360km/h. For the cyclic loading case, no load distribution was applied to allow direct
512 comparisons with earlier published work and to represent a worst-case scenario. The results are
513 summarized as follows:

514 1- The GRS-RW structure showed good performance under both static and cyclic loading
515 comparing to the experiments carried out by Čebašek, et al. (2018), despite the fact the structure
516 was confined on the two lateral sides and the other two were free walls anchored into the fill.

517 2- For each track, more than 3.3 million load cycles were applied. The ballasted track presented
518 a large settlement compared to the slab track, which was approximately 15 times greater in both
519 types of cyclic loading. The magnitude of the plastic strain increment for the cyclic loops at the
520 end and beginning of the loading was only slightly different indicating that the stiffness and
521 density of the substructure had not increased significantly during shakedown.

522 3- The amplitude of the rail displacement under individual cycles at 5.6 Hz and 2.5 Hz loading
523 was approximately 25% lower for the slab track when compared to the case of ballasted track.
524 The major part of the elastic displacement of the rail was caused by the railpad which was about
525 93% for the rail on the slab track and 66% on the ballasted track.

526 4- The amplitude of the sleeper displacement on the ballasted track was approximately 6 to 7
527 times greater than the amplitude of the slab under individual cyclic loading, demonstrating that
528 the vertical and bending track stiffnesses of the slab are much higher than those of the ballasted
529 track, even for a reduced track length.

530 To conclude, the transient displacement and permanent settlement for the case of slab track
531 were significantly lower than those of the ballasted track. Hence, the superior performance of
532 the slab track, which may require less maintenance and thus lead to increased traffic
533 availability. The enhanced inherent quality of the slab track in terms of stability and durability
534 is likely to ensure a smooth ride quality and lower life-cycle costs.

535 **Acknowledgements**

536 The authors are grateful to the Engineering and Physical Sciences Research Council (EPSRC)
537 for funding this work under Grant Numbers EP/N009207/1 and EP/N009215/1. Tensar and
538 Max-Bögl are also acknowledged for their support with regards to the experimental testing
539 stages.

540 **6 References**

- 541 Abadi, T., L. Le Pen, A. Zervos, and W. Powrie. 2016. "A review and evaluation of ballast
542 settlement models using results from the Southampton Railway Testing Facility
543 (SRTF)." *Procedia engineering* 143: 999-1006.
- 544 Alva-Hurtado, J., and E. Selig. 1981. "Permanent strain behavior of railroad ballast."
545 *Proceedings of the International Conference on Soil Mechanics and Foundation*
546 *Engineering* 1: 543-546.
- 547 Berg, R.R., B.R. Christopher, and N.C. Samtani. 2009. *Design of Mechanically Stabilized*
548 *Earth Walls and Reinforced Soil Slopes-Volume II. Report No. FHWA-NHI-10-025.*
549 Washington, D.C: National Highway Institute, Federal Highway Administration.
- 550 Bian, X., H. Jiang, C. Cheng, Y. Chen, R. Chen, and J. Jiang. 2014. "Full-scale model testing
551 on a ballastless high-speed railway under simulated train moving loads." *Soil Dynamics*
552 *and Earthquake Engineering* 66: 368-384.
- 553 Bian, X., Li, W., Qian, Y. and Tutumluer, E., 2020. Analysing the effect of principal stress
554 rotation on railway track settlement by discrete element method. *Géotechnique*, 70 (9),
555 pp.803-821.
- 556 Brown, S., B. Brodrick, N. Thom, and G. McDowell. 2007. "The Nottingham railway test
557 facility, UK." *Proceedings of the Institution of Civil Engineers-Transport* 160 (2): 59-
558 65.
- 559 Čebašek, T. M., A. F. Esen, P. K. Woodward, O. Laghrouche, and D. P. Connolly. 2018. "Full
560 scale laboratory testing of ballast and concrete slab tracks under phased cyclic loading."
561 *Transportation Geotechnics* 17: 33-40.
- 562 Connolly, D.P., Dong, K., Alves Costa, P., Soares, P. and Woodward, P.K., 2020. High speed
563 railway ground dynamics: a multi-model analysis. *International Journal of Rail*
564 *Transportation*, pp.1-23.
- 565 Connolly, D., A. Giannopoulos, and M.C. Forde. 2013. "Numerical modelling of ground borne
566 vibrations from high speed rail lines on embankments." *Soil Dynamics and Earthquake*
567 *Engineering* 46: 13-19.
- 568 Connolly, D.P., G. Kouroussis, P.K. Woodward, P.A. Costa, O. Verlinden, and M.C., Forde.
569 2014. "Field testing and analysis of high speed rail vibrations." *Soil Dynamics and*
570 *Earthquake Engineering*, 67 102-118.
- 571 Dahlberg, T. 2001. "Some railroad settlement models—a critical review." *Proceedings of the*
572 *Institution of Mechanical Engineers, Part F: Journal of Rail and Rapid Transit* 215 (4):
573 289-300.
- 574 Dong, K., D.P. Connolly, O. Laghrouche, P.K. Woodward, and P.A. Costa. 2018. "The
575 stiffening of soft soils on railway lines." *Transportation Geotechnics* 17: 178-191.

- 576 Helwany, S. M. B., J. T.H. Wub, and B. Froessl. 2003. "GRS bridge abutments—an effective
577 means to alleviate bridge approach settlement." *Geotextiles and Geomembranes* 177-
578 196.
- 579 Herold, A. 2005. "Brückenwiderlager aus KBE-Kunststoffbewehrte Erde, Einsatzgebiete Und
580 Anwendungsgrenzen." *Geotechnik-Kolloquium, Freiberg, Technische Institut für*
581 *Geotechnik der Universität Bergakademie Freiberg, Heft* (Geotechnik-Kolloquium,
582 Freiberg, Technische Institut) 195-217.
- 583 Horii, K., H. Kishida, M. Tateyama, and F. Tatsuoka. 1994. "Computerized design method for
584 geosynthetic-reinforced soil retaining walls for railway embankments." *Recent Case*
585 *Histories of Permanent Geosynthetic-Reinforced Soil Retaining Walls* 205-218.
- 586 Indraratna, B., N. T. Ngo, and C. Rujikiatkamjorn. 2012. "Deformation of coal fouled ballast
587 stabilized with geogrid under cyclic load." *Journal of Geotechnical and*
588 *Geoenvironmental Engineering* 139 (8): 1275-1289.
- 589 Kim, D.S., and U.J. Kim. 2016. "Performance Evaluation of a New Type of Abutment with
590 Geosynthetics." *Proceedings of the Third International Conference on Railway*
591 *Technology: Research, Development and*. Stirlingshire, Scotland: Civil-Comp Press.
592 33.
- 593 Koseki, J. 2012. "Use of Geosynthetics to Improve Seismic Performance of Earth Structures."
594 *Geotextiles and Geomembranes* (<http://www.mercerlecture.com/>) 34: 51-68.
595 <http://www.mercerlecture.com/>.
- 596 Koseki, J., R. J. Bathurst, E. Güler, J. Kuwano, and M. Maugeri. 2006. "Seismic stability of
597 reinforced soil walls." *Invited keynote paper, 8th International Conference of*
598 *Geosynthetics, Yokohama* 18-22.
- 599 Koseki, J., Y. Munaf, F. Tatsuoka, M. Tateyama, K. Kojima, and T. Sato. 1996. "Shaking and
600 tilt table tests of geosynthetic-reinforced soil and conventional-type retaining walls."
601 *Geosynthetics international* 73-96.
- 602 Lee, K.Z.Z., and J. T.H. Wu. 2004. "A synthesis of case histories on GRS bridge supporting
603 structures with flexible facing." *Geotextiles and Geomembranes* 181-204.
- 604 Lekarp, F., Isacsson, U. and Dawson, A., 2000. State of the art. I: Resilient response of unbound
605 aggregates. *Journal of transportation engineering*, 126 (1), pp.66-75.
- 606 Lenart, S., M. Kralj, S.P. Medved, and J. Šuler. 2016. "Design and construction of the first
607 GRS integrated bridge with FHR facings in Europe." *Transportation Geotechnics* 8 26-
608 34.
- 609 Powrie, W. ed., 2016. A Guide to Track Stiffness: August 2016. University of Southampton
610 Department of Civil & Environmental Engineering.

- 611 Punetha, P., S. Nimbalkar, and H. Khabbaz. 2020. "Evaluation of additional confinement for
612 three-dimensional geoinclusions under general stress state." *Canadian Geotechnical*
613 *Journal* 57 (3): 453-461.
- 614 Sato, Y. 1995. "Japanese studies on deterioration of ballasted track." *Vehicle system dynamics*
615 24 (1): 197-208.
- 616 Selig, E. T., and J. M. Waters. 1994. *Track geotechnology and substructure management*.
617 Thomas Telford.
- 618 Shenton, M. 1985. "Ballast deformation and track deterioration." *Track technology* 253-265.
- 619 Singh, RP, S. Nimbalkar, S. Singh, and D. Choudhury. 2020. "Field assessment of railway
620 ballast degradation and mitigation using geotextile." *Geotextiles and Geomembranes*
621 48 (3): 275-283.
- 622 Skinner, G. D., and R. K. Rowe. 2005. "Design behaviour of geosynthetic reinforced retaining
623 wall and bridge abutment on yielding foundation." *Geotextiles and Geomembranes*
624 234-260.
- 625 Tatsuoka, F., and K. Watanabe. 2015. "Design, Construction, and Performance of GRS
626 Structures for Railways in Japan." In *Ground Improvement Case Histories*.
627 *Compaction, Grouting and*, 657-692. Elsevier.
- 628 Tatsuoka, F., M. Tateyama, J. Koseki, and T. Yonezawa. 2014. "Geosynthetic-Reinforced Soil
629 Structures for Railways in Japan." *Transp. Infrastruct. Geotech* 3–53.
- 630 Tatsuoka, F., M. Tateyama, T. Uchimura, and J. Koseki. 1997. "Geosynthetic-reinforced soil
631 retaining walls as important permanent structures Geosynthetics international."
632 *Geosynthetics international, Vol. 4, No. 2* 81-135.
- 633 Tatsuoka, F., M. Tateyama, Y. Mohri, and K. Matsushima. 2007. "Remedial treatment of soil
634 structures using geosynthetic-reinforcing technology." *Geotextiles and Geomembranes*
635 204–220.
- 636 Tatsuoka, F. 2019. "Geosynthetic-reinforced soil structures for transportation: from walls to
637 bridges." *Australia New Zealand Conference on Geomechanics, 13th, 2019, Perth,*
638 *Western Australia*. Australia.
- 639 Thom, N., and J. Oakley. 2006. "Predicting differential settlement in a railway trackbed."
640 *Proceedings of Railway foundations conference: Railfound* 6: 190-200.
- 641 Woodward, P., J. Kennedy, O. Laghrouche, D. Connolly, and G. Medero. 2014. "Study of
642 railway track stiffness modification by polyurethane reinforcement of the ballast."
643 *Transportation Geotechnics* 1 (4): 214-224.
- 644 Wu, Jonathan T.H. 2018. *Geosynthetic Reinforced Soil (GRS) Walls*. John Wiley & Sons.

- 645 Yonezawa, T., T. Yamazaki, M. Tateyama, and F. Tatsuoka. 2014. "Design and construction
646 of geosynthetic-reinforced soil structures for Hokkaido high-speed train line."
647 *Transportation Geotechnics* 3-20.
- 648 Yu, Z., D. P. Connolly, P. K. Woodward, and O. Laghrouche. 2019. "Settlement behaviour of
649 hybrid asphalt-ballast railway tracks." *Construction and Building Materials* 208: 808-
650 817.
- 651 Yu, Z., P.K. Woodward, O. Laghrouche, and D.P., Connolly. 2019. "True triaxial testing of
652 geogrid for high speed railways." *Transportation Geotechnics* 100247.
- 653